Suplemento de la Revista Mexicana de Física **1** (2) 12–17 JUNE–JULY 2020

Characterization of an interstitial current model around a cancer nodule using optical tweezers

O. L. Torres-Saucedo[a], B. Morales-Cruzado[b], and F. G. Pérez-Gutiérrez[a]
[a]*Facultad de Ingeniería, Universidad Autónoma de San Luis Potosí, Av. Manuel Nava No. 8, San Luis Potosí, S.L.P. 78290, México.*
e-mail: torressdo@gmail.com; fgperezg@gmail.com
[b]*CONACYT-Universidad Autónoma de San Luis Potosí, Av. Manuel Nava No. 8, San Luis Potosí, S.L.P. 78290, México.*
e-mail: bettiche_1102@yahoo.com.mx

Received 28 January 2020; accepted 11 March 2020

Currently, the process of diagnosis and treatment of a patient with metastatic cancer is highly inefficient due to the complexity of the disease (metastasis is the spread of cancer cells from a primary tumor to secondary tumors at distant sites [1]). However, recent studies have shown that shear stress, caused by natural microfluidic currents, causes cancer cells to break away, spreading them to secondary sites [2] and aggravating the disease. The extent of shear stress on nodules due to microfluidic currents has not been experimentally proven. In the present study, a methodology developed to induce local shear stresses on a cancer nodule model from velocity field measurements is presented. Such methodology is based on the use of the optical tweezers velocimetry technique reported by Eom, *et al*. [3] and Almendarez, *et al*. [4]. The methodology consists on using the holographic optical tweezers velocimetry technique (i.e. multiple trapping in one domain), in order to measure, in a discretized way, the flow field at different positions, and approximate through least squares the velocity profiles; with such information, the shear stresses on the surface of the nodule model will be approximated. The methodology contributes to the understanding of metastasis process and other applications, such as: the development of thrombosis, tumor formation, stopping bleeding, etc.

Keywords: Optical tweezers; laminar flows; flow in channels; steady shear flows; biological fluid dynamics.

PACS: 87.80.Cc; 47.15.-x; 83.50.Ha; 83.50.Ax; 47.60.+i

1. Introduction

Eradicating metastatic cancer is one of the greatest challenges today; it is reported that for all types of cancer, only one out of five patients diagnosed with metastatic cancer will survive more than 5 years [1]. In recent years, it has been shown that metastasis is directly related to shear stress caused by natural microfluidic currents, which result in the shedding of cancer cells to distant sites [2]; however, the magnitude of shear stress causing the shedding of cancer cells has not been reported.

In the present study, a technique developed to approximate shear stresses on a cancer nodule model is presented, so that in future studies, the technique can be used to analyze the behavior of cancer nodules due to the increase or decrease of shear stresses produced by the flow.

To approximate the shear stresses, the velocimetry technique with optical tweezers reported by Eom, *et al*. [3] and Almendarez, *et al*. [4] is used. This technique is based on the fact that the restoring force of optical tweezers can be modeled as a spring, taking care that the optical tweezers are in its linear region (in Fig. 1, it can be seen that the curve has an approximately linear section).

Since the modeling of the optical tweezers is based on a spring, the restitution force of the optical tweezers ($F_{x\text{tweezers}}$) is

$$F_{x\text{tweezers}} = k_x \Delta x. \tag{1}$$

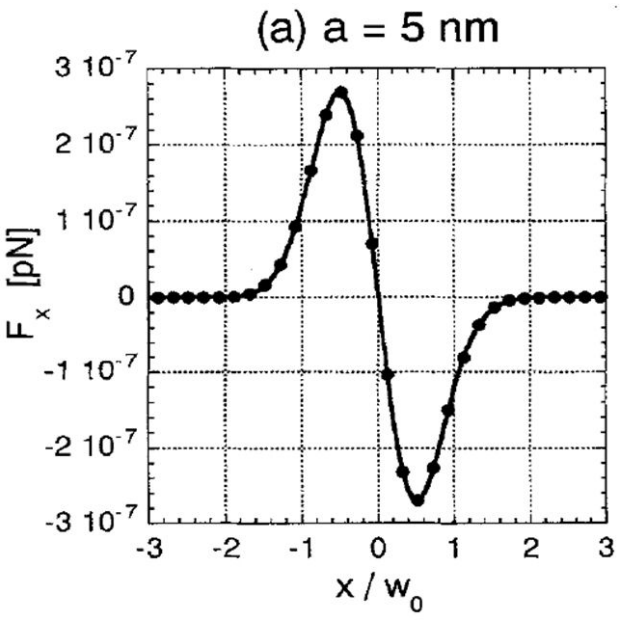

FIGURE 1. Behavior of the optical tweezers, Figure taken from Harada, *et al.,* [5].

Where k_x is the trap stiffness constant of the optical tweezers and Δx is the average displacement of the trapped particle.

According to the equipartition theorem, k_x is determined as follows:

$$k_x = \frac{k_B T}{\langle (x(t) - \bar{x}(t))^2 \rangle}. \quad (2)$$

Where k_B is Boltzman's constant (1.38×10^{-23} J/K), T is the temperature of the fluid, and $\langle (x(t) - \bar{x}(t))^2 \rangle$ is the variance of the particle position.

In turn, the restitution force of the tweezers is equal to the drag force (F_{drag}) suffered by the particle. The drag force is:

$$F_{\text{drag}} = (6\pi\eta a\varepsilon)u. \quad (3)$$

Where η is the dynamic viscosity of the fluid, a is the radius of the particle, u is the velocity of the fluid, and ε is a correction factor that takes into account the external effects produced by the walls of the channel.

The correction factor ε is obtained from Faxen's law shown in Eq. (4).

$$\varepsilon = \frac{1}{1 - \frac{9}{16}\left(\frac{a}{h}\right) + \frac{1}{8}\left(\frac{a}{h}\right)^3 - \frac{45}{256}\left(\frac{a}{h}\right)^4 - \frac{1}{16}\left(\frac{a}{h}\right)^5} + \frac{1}{1 - \frac{9}{16}\left(\frac{a}{t-h}\right) + \frac{1}{8}\left(\frac{a}{t-h}\right)^3 - \frac{45}{256}\left(\frac{a}{t-h}\right)^4 - \frac{1}{16}\left(\frac{a}{t-h}\right)^5}. \quad (4)$$

Where h is the distance to the nearest surface and t is the height of the channel.

From the above, it can be determined that the velocity of the fluid will be

$$u = \frac{k_x \Delta x}{6\pi\eta a\varepsilon}. \quad (5)$$

The methodology consists on using the velocimetry technique described above with optical holographic tweezers (*i.e.* multiple trapping in one domain), in order to discretely measure the flow field at various depths, approximate velocity profiles, from which, the shear stresses on the surface of the nodule model will be calculated.

2. Background

Among the studies that gave the most relevant advances in the development of metastasis by physiological factors, Shields *et al*. [6] using a 3D in vitro culture with four human cell lines immersed in a tumor cell culture flow, showed that the tumor cells follow the direction of the flow, proving that the interstitial flow increases the migratory potential of the cancer cells.

Polacheck *et al.* [7] using a model based on Shields *et al.* [6], showed that the direction of migration of tumor cells depends on the strength of the flow, because chemotaxis (chemotaxis is the phenomenon that causes cells to direct their movements to the concentration of other cells) interposes or assists the direction of flow according to the concentration of cells.

Subsequently, Rizvi *et al*. [2] investigated the role of microfluidic forces as modulators of metastatic cancer development on a microfluidic platform using 3D ovarian cancer nodules; evaluating cancer cultures under laminar and continuous flow. Finding that microfluidic currents make tumors mobile and more aggressive. No results were obtained on the shear stress experienced by the nodules.

In 2016, Ip, *et al.,* [8] approximated the shear stresses on a cancer nodule grown in a microchannel (4 mm wide, 25 mm long, and 250 μm high), finding that a cancer nodule with a diameter of 104.6 ± 167 μm, experienced average shear stresses of 0.00390268 dyn/cm^2 (for a flow rate of 30.1 μl/h) and 0.0390525 dyn/cm^2 (301.2 μl/h), simulated in ANSYS, without having an experimental measurement to confirm the shear stress.

Among the most relevant studies for obtaining shear forces in microfluidic currents are Lu, *et al.* [9], who report a study in which they analyzed how cells are adhered in microchannels, comparing the experimental results with the maximum shear forces suffered by the channel as calculated analytically.

Another similar study is presented by Gutiérrez *et al.* [10], in which the relationship of the shear stresses with the adhesion of platelets to blood vessel walls to stop bleeding is analyzed.

Kohles *et al*. [11] determined the shear stress in a particle suspended in the flow, based on the idea that if shear and normal stresses are proportional to the flow velocity, the maximum stress in a unidirectional flow will be limited by the holding power. This idea is only valid in the case of a suspended particle, because the only force that interacts with the particle (assuming that body forces are neglected), is the flow around the particle, so for an object that obstructs a channel, the balance of forces is different, and it is necessary to contemplate that a certain part of the object is attached to the channel. For the study by Kohles *et al.* [11] the particle image microvelocimetry technique (μVIP) was used. For such research, the velocity resolution was established by an interrogation region size of 16×16 pixels or 1.74×1.74 μm^2, which resulted in the calculation of the stresses introduced by the flow in the vicinity of the suspended sphere and not on the surface of the sphere. Therefore, from the relationship of the drag force suffered by a particle trapped in an optical tweezers and the measurement of the velocity using μVIP, values of normal and shear stresses were determined; this technique is known as μPIVOT and is the combination between particle image microvelocimetry and optical tweezers.

Later, the collaboration of Nève, *et al*. [12], formed by researchers in common with the article by Kohles *et al.* [11], used the μPIVOT technique to determine the biomechanical factors that produce the degradation of tissues, due to the stresses to which it is subjected; this research was carried out with the aim of making advances in the disease of osteoarthritis.

In a similar way, Wu *et al*. [13], using the μPIVOT technique, manage to map in a rectangular microchannel (without

obstacle) the shear stresses.

Currently, no methodology is reported to determine shear stresses on an obstacle attached to a microchannel wall using optical tweezers.

3. Materials and methods

The channel with attached obstacles used in this work was constructed to be 0.06 mm high (bounded by 0.06 mm double-sided tape), 0.5 cm wide, and 4.5 cm long (see Fig. 2).

The procedure used to fabricate the microchannel is described below:

1. A slide was drilled with two holes spaced for the flow in and out.
2. Needles were cut from syringes and attached to the holes made in the slide using epoxy adhesive.
3. Double-sided 0.06 mm thick tape was glued to the slide to form the microchannel.
4. A mixture of salt, particles of 2 μm diameter (zirconium oxide) and Milli Q water was made, in which a coverslip was subsequently dipped.
5. The coverslip was left to dry.
6. The coverslip was glued (dry) to the other side of the slide's adhesive tape.
7. It was sealed around each channel with adhesive to prevent leakage.

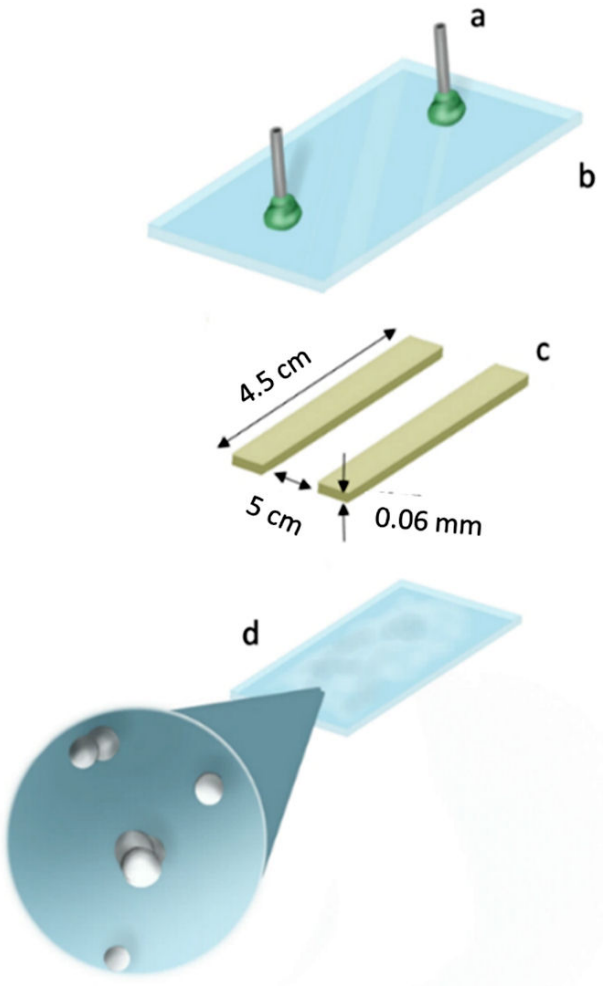

FIGURE 2. Exploded channel view a) needle stuck with epoxy adhesive to a slide, b) slide, c) double-sided tape 0.06 mm thick, d) cover with obstacles stuck.

Some of the obstacles obtained are shown in Fig. 3.

The fluid used was mixture of water with spherical 2 μm in diameter polystyrene particles with concentration of 10 μl of polystyrene particles per 1 ml of water. The mixture was pumped using a kds100 model kdScientific infusion syringe pump at a rate of 3.8×10^{-4} mm^3/s.

To make the holograms, CorelDraw was used to produce images of 5 pixels in diameter (representing the trapping points) with a black background, in an image with screen dimensions of 1920×1080 pixels, which corresponds to the resolution of the spatial light modulator (SLM), which was later converted into a hologram through a Matlab program available in the Light-Matter Interaction laboratory, at the UASLP.

Figure 4 shows a schematic of the optical tweezers setup used. Microparticle trapping was archived producing an optical tweezer using 532 mm wavelength, continuous wave laser (Opus532 of Quantum Laser). The laser beam was widened to overfill the Liquid Crystal on Silicon (LCOS) display of the SLM (LETO model by Holoeye) with resolution of 1920×1080 pixels. Then, the beam is reflected on a dichroic mirror with a cut-off length of 605 nm (Thorlabs DMLP605) and finally focused through a 100x oil immersion, NA=1.25, 0.23 mm working distance, microscope objective (Nikon). Such microscope objective, along with

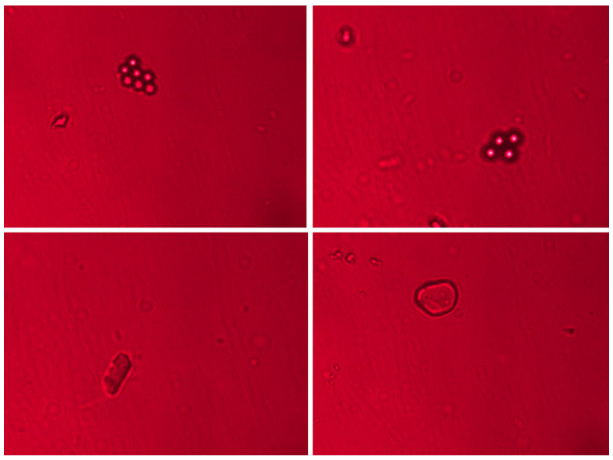

FIGURE 3. Screenshots of obstacles obtained in a microchannel.

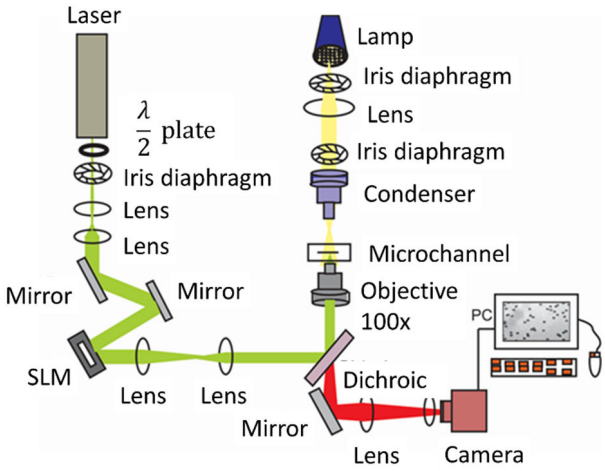

FIGURE 4. Diagram of the optical tweezers arrangement used by the light interaction with materials laboratory in the UASLP.

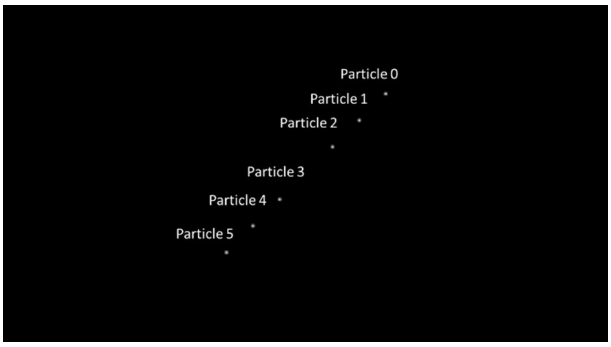

FIGURE 5. Image of the diagonal distribution of trapping points.

the illumination system consisting on the white light tungsten lamp (Thorlabs' QTH10) and a condenser, were used to form the image of the trapping zone on the camera.

For trapping depth positioning, TPZ001 modules (Thorlabs) were used to control the direction, feed back with a TSG001 position sensor connected to the base (from Thorlabs) to improve accuracy.

The experiments were performed at a temperature of 20°C.

For the measurement of the flow field, a 6-particle trapping hologram was used with a hole in the central part where the obstacle will be located, the locations of the particle trapping along with its numbering are shown in Table I and Fig. 5.

TABLE I. Position of trapped particles.

Particle	Coordinates (pixels)
0	884.7, 141.2
1	809.0, 263.6
2	733.4, 388.6
3	584.5, 634.9
4	507.5, 763.4
5	432.8, 887.4

TABLE II. Stiffness constants of the optical tweezers in various locations.

depth (μm)	particle	k_x (pN/μm)	k_y (pN/μm)	Error (pN/μm)	Error (pN/μm)
5	0	0.564	0.017	0.397	0.004
5	1	1.734	0.094	1.154	0.166
5	2	1.836	0.213	1.422	0.263
5	3	3.313	0.295	1.662	0.227
5	4	2.190	0.197	1.293	0.206
5	5	1.145	0.065	0.810	0.145
7	0	0.529	0.032	0.378	0.026
7	1	1.751	0.064	1.247	0.093
7	2	1.923	0.101	1.500	0.161
7	3	2.754	0.324	1.769	0.132
7	4	1.977	0.061	1.334	0.142
7	5	1.039	0.068	0.782	0.026
9	0	0.574	0.004	0.334	0.021
9	1	1.686	0.082	1.366	0.097
9	2	1.924	0.125	1.653	0.148
9	3	2.714	0.280	1.854	0.106
9	4	1.958	0.088	1.387	0.067
9	5	1.102	0.126	0.909	0.117

For velocimetry, it is necessary to obtain the stiffness constants and the average position of the particles with and without flow, using Eq. (2). Raw data for this calculation were collected from 3 videos with and without flow recorded with 300 frames each, positioning the trapped particle 5, 7, and 9 μm deep. Such videos were processed through the algorithm developed by Crocker and Grier [14]. Finally the speed of the particles was calculated using Eq. (5).

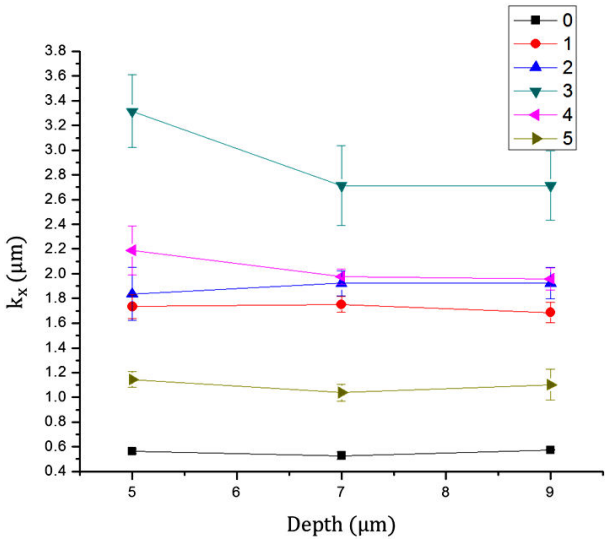

FIGURE 6. Stiffness constants in the x-direction of the particles at various depths

To obtain the shear stresses, a no slip boundary condition was added to the surface of all trapped particles. Later, with the velocities and the boundary condition, velocity distribution were approximated using least squares fit to a quadratic function. With the curves obtained and Eq. (6) (evaluated at $y =$ surface), the shear stresses on the wall where the obstacle was attached were approximated.

$$\tau = \mu \frac{du}{dy}(y = \text{surface}). \tag{6}$$

Where τ is the shear stress, u is the velocity of the fluid and μ is the dynamic viscosity.

4. Results and discussion

The methodology used allowed to approximate the shear stresses on the wall of the channel where the obstacle was attached, however, the trapped particles were far from the obstacle, therefore the shear stresses obtained are on the channel surface within the vicinity of the obstacle and not on the obstacle surface.

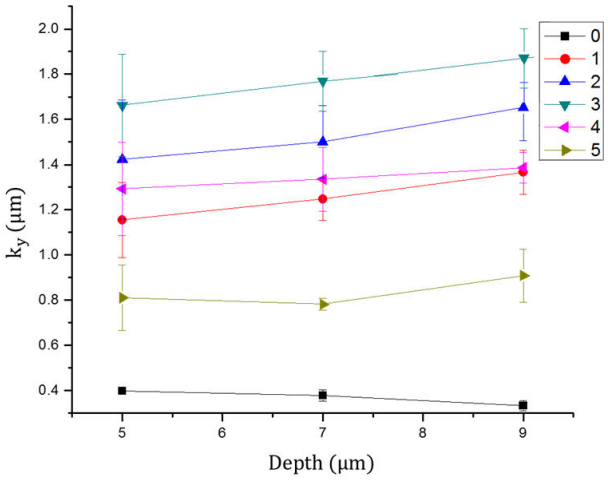

FIGURE 7. Stiffness constants in direction and of the particles at various depths.

TABLE III. Average displacements of particles.

Particle/ Depth	5 μm	7 μm	9 μm
0	1.574 μm	1.738 μm	2.338 μm
1	–	0.159 μm	0.453 μm
2	0.375 μm	0.410 μm	0.666 μm
3	0.355 μm	0.749 μm	–
4	0.446 μm	0.570 μm	0.741 μm
5	0.807 μm	0.926 μm	1.170 μm

The stiffness constants of the optical tweezers for various particles at the different depths are shown in Table II and Figs. 6 and 7.

The average particle displacements due to flow and discrete point velocities are shown in Tables III and IV (the gaps are due to unacceptable experimental data because a bacterium was detected interacting with the trapped particle).

Figure 8 shows the particle velocities at different depths and the approximate curves to the discrete points. The velo-

TABLE IV. Velocimetry in the discrete points.

Particle/ Depth	0 μm	5 μm	7 μm	9 μm
0	0 μm/s	2.579 μm/s	2.712 μm/s	3.219 μm/s
1	0 μm/s	–	0.817 μm/s	2.552 μm/s
2	0 μm/s	2.202 μm/s	2.536 μm/s	4.545 μm/s
3	0 μm/s	2.432 μm/s	5.470 μm/s	–
4	0 μm/s	2.381 μm/s	3.139 μm/s	4.236 μm/s
5	0 μm/s	2.696 μm/s	2.987 μm/s	4.388 μm/s

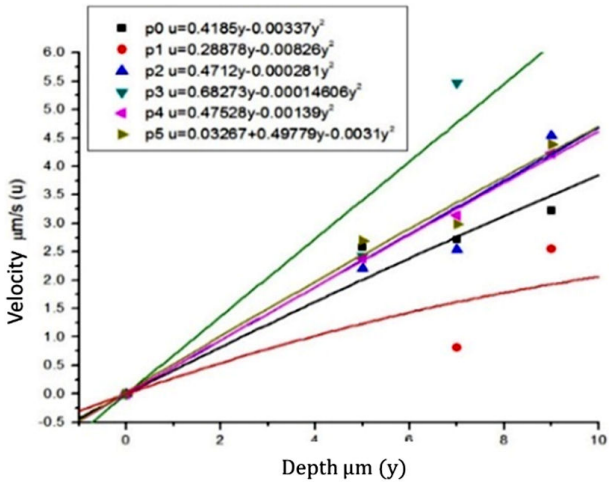

FIGURE 8. Velocities of particles at different depths.

TABLE V. Results of shear stresses.

Shear stresses
$\tau_{p0} = 3.738 \times 10^{-4}$ N/m^2
$\tau_{p1} = 2.579 \times 10^{-4}$ N/m^2
$\tau_{p2} = 4.208 \times 10^{-4}$ N/m^2
$\tau_{p3} = 6.097 \times 10^{-4}$ N/m^2
$\tau_{p4} = 4.244 \times 10^{-4}$ N/m^2
$\tau_{p5} = 4.445 \times 10^{-4}$ N/m^2

city as a function of depth obeys a parabola because the walls of the channel are fixed as expected. Figure 8 shows that the velocities correspond only to a small section of parabola because the measurements were made at a maximum depth of 9 μm and the total depth of the channel is approximately 60 μm.

Using the equations found in Fig. 8 and Eq. (6), it is obtained that the shear forces will be

As can be seen in Table V, the shear stresses in the central zone are higher due to the proximity to the obstacle, the next two on each side are similar and lower as expected.

Although the results are preliminary, they show a physically correct tendency.

5. Conclusions

- The fluid velocity profiles obtained, as a function of depth, showed the behavior predicted by the theory.
- The velocities of each trapped particle showed similar behavior, due to the remoteness of the obstacle.
- The approximation of the shear stresses was physically acceptable because these are maximums in the vicinity of the obstacle, however, these are still preliminary results.
- The hologram used trapped particles too far away from the obstacle, so holograms will be implemented in the form of rings, to adapt to different circumferences, in order to approximate the shear forces in the vicinity of the obstacle.

Acknowledgments

The authors are grateful for the support of CONACyT Mexico through grant A1-S-9887.

1. A. Schroeder *et al*., Treating metastatic cancer with, *Nat. Rev. Cancer* **12** (2012) 39. https://doi.org/10.1038/nrc3180
2. I. Rizvi *et al*., 'Flow induces epithelial-mesenchymal transition, cellular heterogeneity and biomarker modulation in 3D ovarian cancer nodules, *PNAS* **110** (2013) E1974-E1983. https://doi.org/10.1073/pnas.1216989110
3. N. Eom, V. Stevens, A. B. Wedding, R. Sedev and J. N. Connor, Probing fluid flow using the force measurement capability of optical trapping., *Adv. Powder Techno.* **25** (2014) 1249-1253. https://doi.org/10.1016/j.apt.2014.06.023
4. P. Almendarez-Rangel, *Implementación de un sistema de medición de velocidad con aplicación en microfluidos basado en el uso de pinzas ópticas* (Tesis de maestría), (San Luis Potosí, 2017).
5. Y. Harada and T. Asakura, Radiation forces on a dielectric sphere in the Rayleigh scattering regime, *Opt. Commun.* **124** (1996) 529-241. https://doi.org/10.1016/0030-4018(95)00753-9
6. J. D. Shields, M. E. Fleury, C. Yong, A. A. Tomei, G. J. Randolph and M. A. Swartz, Auntologous chemotaxis as a mechanism of tumor cell homing to lymphatics via interstitial flow and autocrine CCR7 signaling, *Cancer cell* **11** (2007) 526-538. https://doi.org/10.1016/j.ccr.2007.04.020
7. W. J. Polacheck, J. L. Charest and R. D. Kamm, Interstitial flow influences direction of tumor cell migration through competing mechanisms, *PNAS* **108** (2011) 11115-11120. https://doi.org/10.1073/pnas.1103581108
8. C. K. Ip, S. S. Li, M. Y. Tang, H. C. Shum and A. S. Wong, Stemness and chemoresistance in epithelial ovarian carcinoma cells under shear stress. *Sci. Rep.* **6** (2016) 26788. https://doi.org/10.1038/srep26788
9. H. Lu, L. Y. Koo, W. M. Wang, D. A. Lauffenburger, L. G. Griffith and K. F. Jensen, Microfluidic shear devices for quantitive analysis of cell adhesion, *Anal. Chem.* **76** (2004) 5257-5264. https://doi.org/10.1021/ac049837t
10. E. Gutiérrez, B. G. Petrich, S. J. Shattil, M. H. Ginsberg, A. Groisman and A. Kasirer-Friede, Microfluidic devices for studies of shear-dependent platelet adhesion, *Lab chip* **8** (2008) 1486-1495. https://doi.org/10.1039/B804795B
11. S. S. Kohles, N. Néve, J. D. Zimmerman and D. C. Tretheway, Mechanical stress analysis of microfluidic enviroments designed for isolated biological cell investigations, *J. Biomech. Eng.* **131** (2009) 121006. https://doi.org/10.1115/1.4000121
12. N. Néve, S. S. Kohles, S. R. Winn and D. C. Tretheway, Manipulation of suspended single cells by microfluidics and optical tweezers, *Cel. Mol. bioeng.* **3** (2010) 213-228. https://doi.org/10.1007/s12195-010-0113-3
13. J. Wu, D. Day and M. Gu, Shear stress maping in microfluidic devices by optical tweezers, *Opt. Express* **18** (2010) 7611-7616. https://doi.org/10.1364/OE.18.007611
14. J. C. Crocker and D. G. Grier, Methods of Digital Video Microscopy for Colloidal Studies, *J. Colloid and Inter. Scie*. **179** (1995) 298-310. https://doi.org/10.1006/jcis.1996.0217